RSC Advances

PAPER

View Article Online
View Journal | View Issue

Open Access Article. Published on 04 May 2023. Downloaded on 1/18/2026 3:06:55 PM.
This article is licensed under a Creative Commons Attribution-NonCommercial 3.0 Unported Licence.

Cite this: *RSC Adv.*, 2023, **13**, 13683

Ag NPs decorated on the magnetic rod-like hydroxyapatite/MIL-101(Fe) nanocomposite as an efficient catalyst for the reduction of some nitroaromatic compounds and as an effective antimicrobial agent

Maryam Beiranvand,[a] Saeed Farhadi *[a] and Abdelnasser Mohammadi-Gholami[b]

Received 21st February 2023
Accepted 24th April 2023

DOI: 10.1039/d3ra01180a

rsc.li/rsc-advances

A rod-like magnetic nanocomposite was successfully synthesized in this work by loading Ag and Fe_3O_4 nanoparticles onto the surface of the hydroxyapatite/MIL-101(Fe) metal–organic framework. Various techniques were used to investigate the crystalline nature, size, morphology, and magnetic and structural properties of the HAP/MIL-101(Fe)/Ag/Fe_3O_4 nanocomposite, including X-ray diffraction (XRD), Fourier transform infrared (FT-IR) spectroscopy, Raman spectroscopy, field-emission scanning electron microscopy (FE-SEM), energy-dispersive X-ray spectroscopy (EDX), transmission electron microscopy (TEM), vibrating sample magnetometry (VSM), BET surface area measurements, and zeta potential analysis. The results indicate that the nanocomposite sample is composed of Ag and Fe_3O_4 nanoparticles adhered to rod-like hydroxyapatite/MIL-101(Fe). The catalytic and antibacterial abilities of the as-prepared HAP/MIL-101(Fe)/Ag/Fe_3O_4 were studied. This nanocomposite was utilized as a heterogeneous catalyst for the catalytic reduction of toxic pollutants, including 4-nitrophenol (4-NP), 2-nitrophenol (2-NP), 2,4-dinitrophenol (2,4-NP), 4-nitroaniline (4-NA), and 2-nitroaniline (2-NA) by $NaBH_4$ in water and at room temperature. These compounds were converted to their amine derivatives within 8–18 min with rate constant values equal to 0.2, 0.3, 0.33, and 0.47 min^{-1}, respectively. This quaternary magnetic catalyst can be easily separated from the reaction medium using an external magnetic field and reused. The synthesized nanocomposite maintained its efficiency in reducing nitroaromatic compounds after 5 runs, showing the high stability of the catalyst. Besides, the antibacterial activity of the nanocomposite against Gram-negative and Gram-positive bacteria was evaluated using the disk diffusion method. The inhibition zone diameter of the nanocomposite against *Staphylococcus aureus*, *Staphylococcus saprophyticus*, and *Escherichia coli* was measured to be 17, 14, and 12 mm, respectively.

1. Introduction

The pollution of water resources is one of the greatest environmental challenges due to its adverse effects on the health of humans and other living organisms. In recent years, organic pollutants in the environment have caused enormous problems. Organic pollutants, include nitroaromatic compounds, chemicals, organic dyes, pharmaceuticals, and polychlorinated biphenyls, and among them, nitroaromatic compounds have received special attention.[1] Nitroaromatic compounds are widely used in various industries for the manufacture of rubber, fungicides, insecticides, industrial solvents, explosives, *etc.*[2] They can cause irreversible effects on the health of humans, plants, and animals, even at very low concentrations. They display high stability and solubility in water, leading to slow biodegradation, potential toxicity, and mutagenic and carcinogenic effects.[3] Among them, 4-nitrophenol (4-NP) has been reported as a priority toxic contaminant by the United States Environmental Protection Agency (EPA).[4–6] Nitrophenols are one of the most common contaminants existing in various industrial sewages due to their environmental stability and non-biodegradability. Inhalation or skin contact with nitrophenols causes headaches, cyanosis, confusion, stomach, and irritation in the eyes.[7] They also cause damage to the human blood, kidneys, pancreas, central nervous system, liver, and muscles.[8–11] Therefore, the elimination of such toxic contaminants from water and industrial sewages is critical for environmental health, specifically the ecosystem. However, the toxicity of nitrophenols can be minimized by converting them into less toxic and useful species in the aqueous medium, namely, aminophenols. On the other hand, aminophenols are applied as significant intermediates in the manufacture of

---

[a] *Department of Inorganic Chemistry, Faculty of Chemistry, Lorestan University, Khorramabad, 68151-44316, Iran. E-mail: farhadi.s@lu.ac.ir*

[b] *Department of Biology, Lorestan University, Khorramabad, 68151-44316, Iran*

© 2023 The Author(s). Published by the Royal Society of Chemistry

Open Access Article. Published on 04 May 2023. Downloaded on 1/18/2026 3:06:55 PM. This article is licensed under a Creative Commons Attribution-NonCommercial 3.0 Unported Licence.

many pharmaceuticals (paracetamol, acetaminophen, acetanilide, ibuprofen, *etc.*), polymers, antioxidants, hair-dyeing, cosmetics, stabilizers, varnishes, surfactants, and plasticizers.[12–15] Many techniques for the reduction of nitrophenols have been reported, including metal/acid reduction, electrolytic reduction, and chemical reduction. Among reported techniques for this conversion, the chemical reduction of nitrophenols using sodium borohydride ($NaBH_4$) is an efficient, simple, and safe method. The disadvantage of this method is the long reaction time. Therefore, it needs the support of a catalyst to reduce the reaction time. Noble metals and non-noble metals have been used to catalyze this reaction.[16,17] Noble metals reported for the reduction of nitrophenols to aminophenols are metals such as Au, Ag, Pt, Pd, and Ru.[18] However, the high costs of noble metals, scarce resources, and recyclability limit their applications in industry. Among non-noble metals, magnetic nanoparticles such as Fe, Co, and Ni have received considerable attention due to magnetic separability, high catalytic activity, and low costs.[17] However, magnetic nanoparticles are not very stable and easily agglomerate, decreasing their catalytic activity.[17] An effective approach to overcome this problem is to immobilize noble metals on supports with high surface area.[19] In this regard, various supports, such as metal–organic frameworks, alumina, carbon nanotubes, and resins, have been studied. These supports have high catalytic activity, large surface area, and ease of surface modification, making them a suitable option for many environmental applications.

Hydroxyapatite (HAP) is one of the most effective supports with the chemical formula of $Ca_{10}(PO_4)_6(OH)_2$. HAP has been employed in various fields, including drug delivery, gene transfer, and tissue engineering, due to its outstanding characteristics like bioactivity, osteoconductivity, nontoxicity, and biological compatibility with cells and tissues of the human body.[20,21] In addition, HAP has many advantages, such as stability, high adsorption capacity, and modifiable surface groups, which lead to the immobilization of active species on its surface.[22] A special feature of HAP is its ability to accept a large number of anionic and cationic substituents that can help immobilize the nanocatalysts. Therefore, it facilitates the separation and recycling process of immobilized nanocatalysts. Pristine HAP shows low antibacterial properties. Hence, modification of HAP by doping with bacteriostatic metals such as Cu, Ag, and Au can solve this problem.[23]

In recent years, metal–organic frameworks (MOFs) have attracted much attention owing to their unique properties, such as biocompatibility, high specific surface area, high distribution of metallic centers, mechanical stability, high porosity, chemically-tunable structures, and low density. Because of these advantages, MOFs have been applied as a promising material in various applications, including gas storage/separation, drug delivery, fuel cells, catalysis, batteries, sensors, supercapacitors, and luminescence.[24–29]

In the present work, we aimed to synthesize a new magnetic nanocomposite based on HAP and a MOF containing silver nanoparticles (Ag NPs) with high catalytic and antibacterial activities. The catalytic activity of the HAP/MIL-(Fe)/Ag/Fe_3O_4 nanocomposite as a magnetically separable heterogeneous catalyst was evaluated through the reduction of 4-nitrophenol (4-NP), 2-nitrophenol (2-NP), 2,4-dinitrophenol (2,4-NP), 4-nitroaniline (4-NA), and 2-nitroaniline (2-NA) with $NaBH_4$ in aqueous medium and at room temperature. Then, the antibacterial activity of this nanocomposite was tested against three bacteria: *Staphylococcus aureus*, *Staphylococcus saprophyticus*, and *Escherichia coli*.

2. Experimental

2.1. Materials

Diammonium hydrogen phosphate ($(NH_4)_2HPO_4$, 98.5%), sodium hydroxide (NaOH, 98%), calcium nitrate tetrahydrate ($Ca(NO_3)_2\cdot4H_2O$, 98%), ammonium iron(II) sulfate hexahydrate ($(NH_4)_2Fe(SO_4)_2\cdot6H_2O$, 98%), iron(III) chloride ($FeCl_3\cdot6H_2O$, 99%), dimethylformamide (DMF, 99%), terephthalic acid (H_2BDC, 98%), ammonium iron(III) sulfate ($(NH_4)Fe(SO_4)_2\cdot12H_2O$, 98%), ammonium hydroxide (NH_4OH, 25%), silver nitrate ($AgNO_3$, 98%), 4-nitrophenol (98%), 2-nitrophenol (99%), 2,4-dinitrophenol (98%), 4-nitroaniline (98%), 2-nitroaniline (99%), sodium borohydride ($NaBH_4$, 98%), and sodium citrate ($Na_3C_6H_5O_7$, 98%) were used for the synthesis of samples and obtained from Merck.

2.2. Synthesis of hydroxyapatite (HAP) nanorods

HAP powder was synthesized by the following steps: Briefly, $Ca(NO_3)_2\cdot4H_2O$ (15 mL, 0.2 M) and $(NH_4)_2HPO_4$ (15 mL, 0.12 M) aqueous solutions were prepared separately with a stoichiometric ratio of Ca/P = 1.67. Then, $(NH_4)_2HPO_4$ solution was added dropwise to $Ca(NO_3)_2\cdot4H_2O$ solution under magnetic stirring. The pH of the solution was constantly adjusted to 10 by adding 1 M NaOH aqueous solution during the reaction. After sonication for 30 min, the homogenized suspension was transferred into a 50 mL Teflon-lined autoclave and heated at 180 °C for 24 h. The resultant white precipitate was filtered, washed with distilled water to eliminate the remaining NH_4NO_3, and dried at room temperature for 24 h.

2.3. Synthesis of Fe_3O_4 nanoparticles

Fe_3O_4 magnetic nanoparticles were prepared by the co-precipitation method. Briefly, 0.964 g $(NH_4)Fe(SO_4)_2\cdot12H_2O$ and 0.392 g $(NH_4)_2Fe(SO_4)_2\cdot6H_2O$ were dissolved in 30 mL distilled water. Then, 10 mL NH_4OH was added to the solution, adjusting the pH of the solution to 10–11. This mixed solution was stirred for 1 h at 80 °C. The black colored solid product was separated with a magnet and then washed with ethanol and distilled water and dried at 60 °C in an oven.

2.4. Synthesis of Ag nanoparticles (Ag NPs)

Aqueous solutions of sodium citrate (20 mL, 0.6 M), silver nitrate (20 mL, 0.1 M), and sodium hydroxide (20 mL, 0.1 M) were poured into a beaker. Then, an aqueous solution including iron(II) ammonium sulfate (20 mL, 0.3 M) was slowly added to the solution under stirring and reacted for 1 h. The resultant

© 2023 The Author(s). Published by the Royal Society of Chemistry

Open Access Article. Published on 04 May 2023. Downloaded on 1/18/2026 3:06:55 PM.
This article is licensed under a Creative Commons Attribution-NonCommercial 3.0 Unported Licence.

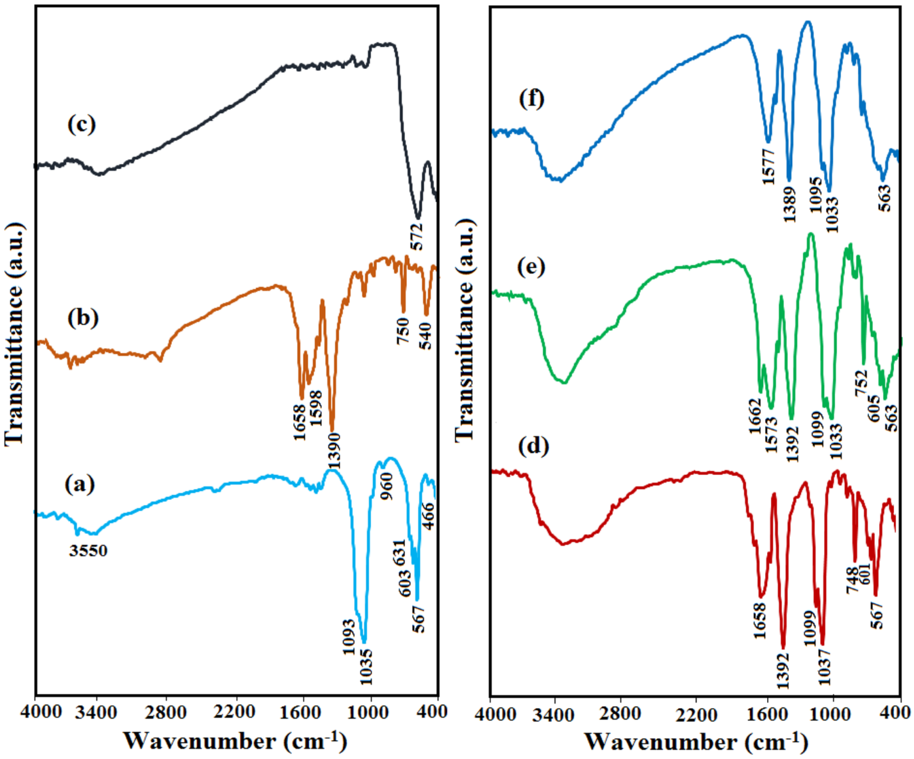

Fig. 1 FT-IR spectra of (a) pure HAP, (b) MIL-101(Fe), (c) Fe_3O_4, (d) HAP/MIL-101(Fe), (e) HAP/MIL-101(Fe)/Ag and (f) HAP/MIL-101(Fe)/Ag/Fe_3O_4 nanocomposite.

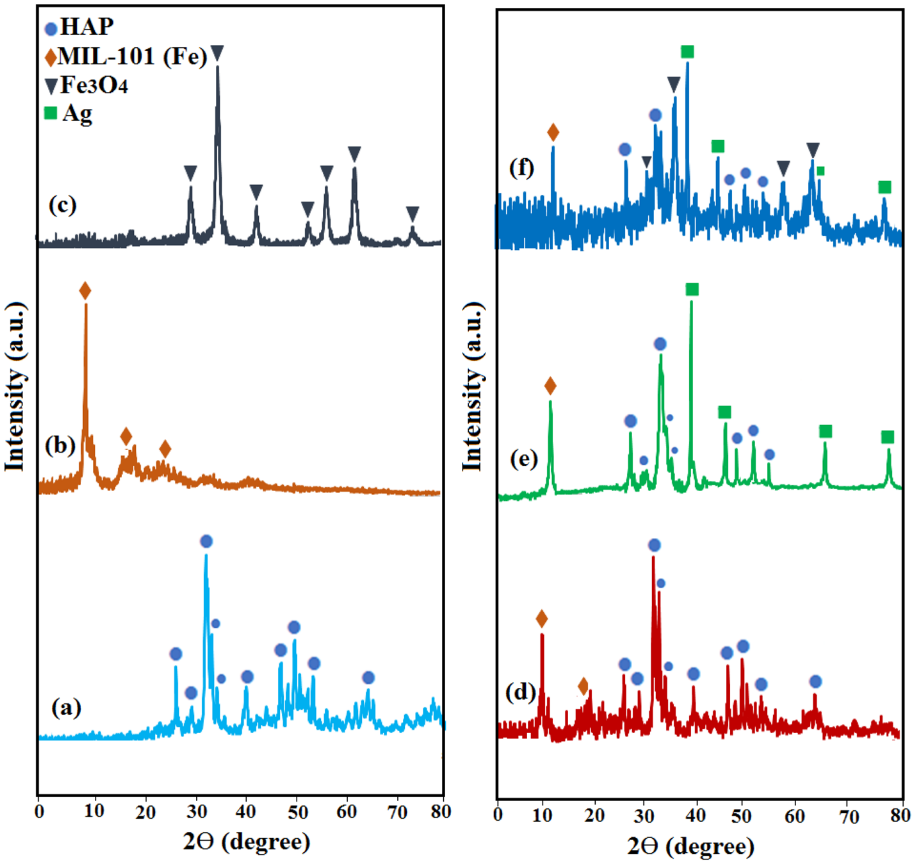

Fig. 2 XRD patterns of (a) pure HAP, (b) MIL-101(Fe), (c) Fe_3O_4, (d) HAP/MIL-101(Fe), (e) HAP/MIL-101(Fe)/Ag, and (f) HAP/MIL-101(Fe)/Ag/Fe_3O_4 nanocomposite.

Open Access Article. Published on 04 May 2023. Downloaded on 1/18/2026 3:06:55 PM.
This article is licensed under a Creative Commons Attribution-NonCommercial 3.0 Unported Licence.

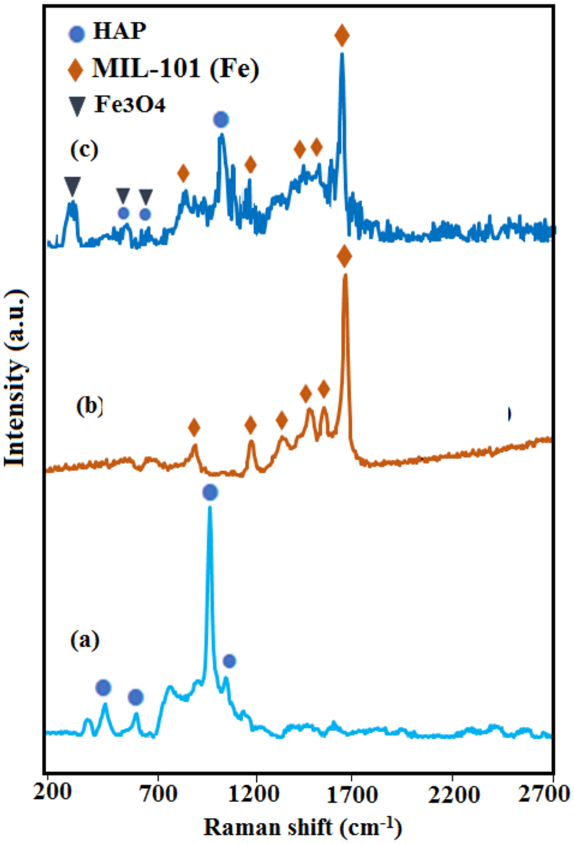

Fig. 3 Raman spectra of (a) pure HAP, (b) MIL-101(Fe), and (c) HAP/MIL-101(Fe)/Ag/Fe_3O_4 nanocomposite.

precipitate was isolated by centrifugation, washed frequently with ethanol, and then dried.

2.5. Synthesis of MIL-101(Fe), HAP/MIL-101(Fe) and HAP/MIL-101(Fe)/Ag samples

The samples of MIL-101(Fe), HAP/MIL-101(Fe), and HAP/MIL-101(Fe)/Ag were prepared through a hydrothermal procedure. 0.2 g of the as-prepared HAP powder, 0.332 g H_2BDC, and 0.8 g $FeCl_3 \cdot 6H_2O$ were dispersed in 30 mL DMF by ultrasonic treatment for 15 min. After that, as prepared Ag NPs (0.125 g) were added to the solution and then stirred for 1 h; the mixture was transferred into a 50 mL Teflon-lined autoclave and warmed at 120 °C for 20 h. The resultant precipitate was filtered, washed with DMF and ethanol several times, and dried at 60 °C for 2 h. Similar processes were also performed to synthesize pure MIL-101(Fe) and HAP/MIL-101(Fe) without the addition of HAP powder and Ag NPs, respectively.

2.6. Synthesis of HAP/MIL-101(Fe)/Ag/Fe_3O_4 nanocomposite

To synthesize HAP/MIL-101(Fe)/Ag/Fe_3O_4 nanocomposites, 0.5 g of dried HAP/MIL-101/Ag powder was dissolved in 15 mL of distilled water. After that, 0.125 g of dried Fe_3O_4 powder was dispersed in 10 mL of distilled water with sonication for 15 min. Then, these two suspensions were mixed. The obtained mixture was stirred for 1 h at ambient temperature. The obtained HAP/MIL-101(Fe)/Ag/Fe_3O_4 nanocomposite product was washed with distilled water and dried at 60 °C for 2 h. The weight percentage values of HPA, MIL-101(Fe), Ag NPs, and Fe_3O_4 components in the nanocomposite based on consumed starting materials were calculated to be 40%, 20%, 25%, and 15%, respectively. HAP is the main component of the composite. The ICP-AES results indicated that the loading amount of Ag in the as-prepared nanocomposite is about 24.85 wt%.

2.7. Characterization

A Fourier transform infrared (Shimadzu-8400S, Japan) spectrometer was used for the FT-IR analysis of the samples. X-ray diffraction (XRD) was employed to evaluate the crystalline phase of the samples by X-ray diffractometer (Philips, 8440, Netherlands) at a voltage of 40 kV. Raman microscope (Model: SENTERRA, Germany) with a laser wavelength of 785 nm was utilized to obtain the Raman spectrum of the samples. The UV-visible absorption spectra of the nitroaromatic compound solutions were recorded using a Cary 100 Varian spectrophotometer. Scanning electron microscopy (FESEM, Mira3, TESCAN) and transmission electron microscopy (TEM, Philips CM120) were used to determine the dimensions as well as the morphology of the samples. The chemical composition of the synthesized nanocomposite was determined using energy dispersive X-ray spectroscopy (EDX). The vibrating sample magnetometer (VSM, Magnetic Daneshpajoh Kashan Co., Iran) was employed for the magnetic measurements at room temperature. Nitrogen adsorption–desorption experiments were performed to check the porosity and specific surface area of the prepared samples using a BELSORP mini apparatus at 77 K. The particle size distribution and zeta potential of the samples were evaluated using a Zetasizer instrument (Malvern, UK) at room temperature.

2.8. Catalytic reduction tests

The reduction of 4-NP was investigated using $NaBH_4$ over the HAP/MIL-101(Fe)/Ag/Fe_3O_4 nanocomposite at room temperature. For this work, 0.5 mL of fresh aqueous solution of $NaBH_4$ with a concentration of 20 mM was mixed with a solution of 4-NP (2 mL, 0.2 mM) in the quartz cell. Then, a selected amount of HAP/MIL-101(Fe)/Ag/Fe_3O_4 nanocatalyst (*e.g.*, 5 mg) was added to the solution, and the UV-vis spectrophotometer was used to record the progress of the reduction process in the range of 200–800 nm. The effect of the nanocatalyst dosage (2.5, 5, 7.5, and 10 mg) was tested on the 4-NP reduction. The reduction process of other nitro compounds was also evaluated under similar conditions.

2.9. Antibacterial activity tests

Disk diffusion method was carried out to measure the antibacterial activity of HAP/MIL-(Fe)/Ag/Fe_3O_4 nanocomposite and Ag NPs against *Escherichia coli*, *Staphylococcus saprophyticus*, and *Staphylococcus aureus* bacteria. The bacteria were cultured in the nutrient agar medium for 24 h at 37 °C before the test and then mixed in 10 mL of saline solution with a wire loop to prepare a suspension similar to the McFarland standard.

© 2023 The Author(s). Published by the Royal Society of Chemistry

Open Access Article. Published on 04 May 2023. Downloaded on 1/18/2026 3:06:55 PM.
This article is licensed under a Creative Commons Attribution-NonCommercial 3.0 Unported Licence.

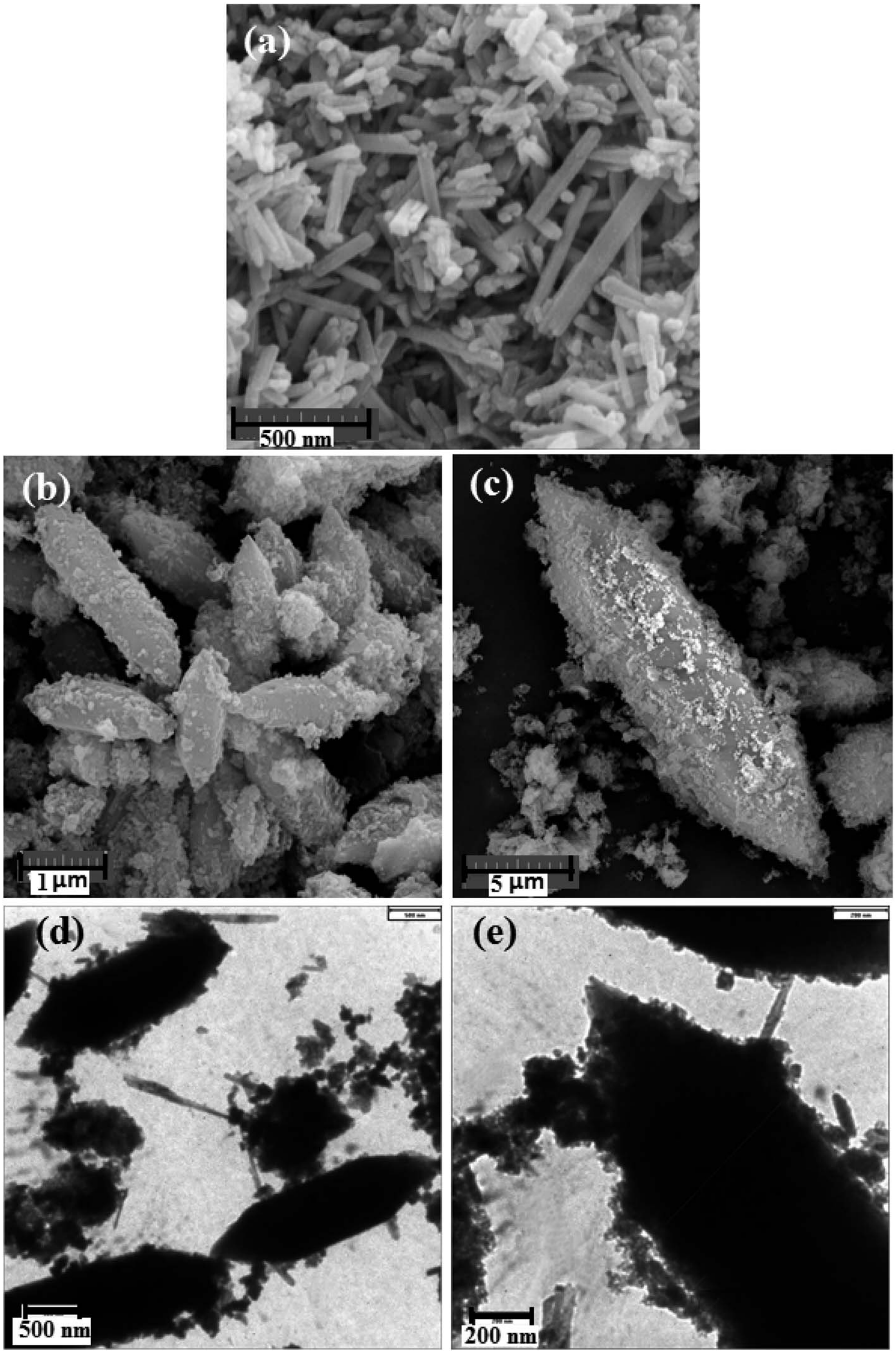

Fig. 4 SEM images of (a) pure HAP, (b and c) HAP/MIL-101(Fe)/Ag/Fe_3O_4 nanocomposite, and (d and e) TEM images of HAP/MIL-101(Fe)/Ag/Fe_3O_4 nanocomposite.

Standardized suspension of each bacterium was inoculated by cotton swab on the surface of nutrient agar plates under sterile conditions. Prepared samples were dissolved in water, and the sterile blank discs were saturated with 40 μl of each sample. Discs containing samples were placed onto nutrient agar plates and amikacin was used as a positive control. The plates were incubated for 24 h at 37 °C. These tests for each bacterial strain were performed three times, and the average inhibition zone diameter was reported in millimeters.

3. Results and discussion

3.1. Characterization of the HAP/MIL-101(Fe)/Ag/Fe_3O_4 nanocomposites

The functional groups in the pure HAP, MIL-101(Fe), Fe_3O_4, HAP/MIL-101(Fe), HAP/MIL-101(Fe)/Ag, and HAP/MIL-101(Fe)/Ag/Fe_3O_4 nanocomposite were recognized *via* FT-IR analysis and the corresponding spectra are plotted in Fig. 1. In the HAP spectrum (Fig. 1(a)), the sharp peaks at 1035, 1093 cm^{-1} were

Open Access Article. Published on 04 May 2023. Downloaded on 1/18/2026 3:06:55 PM.
This article is licensed under a Creative Commons Attribution-NonCommercial 3.0 Unported Licence.

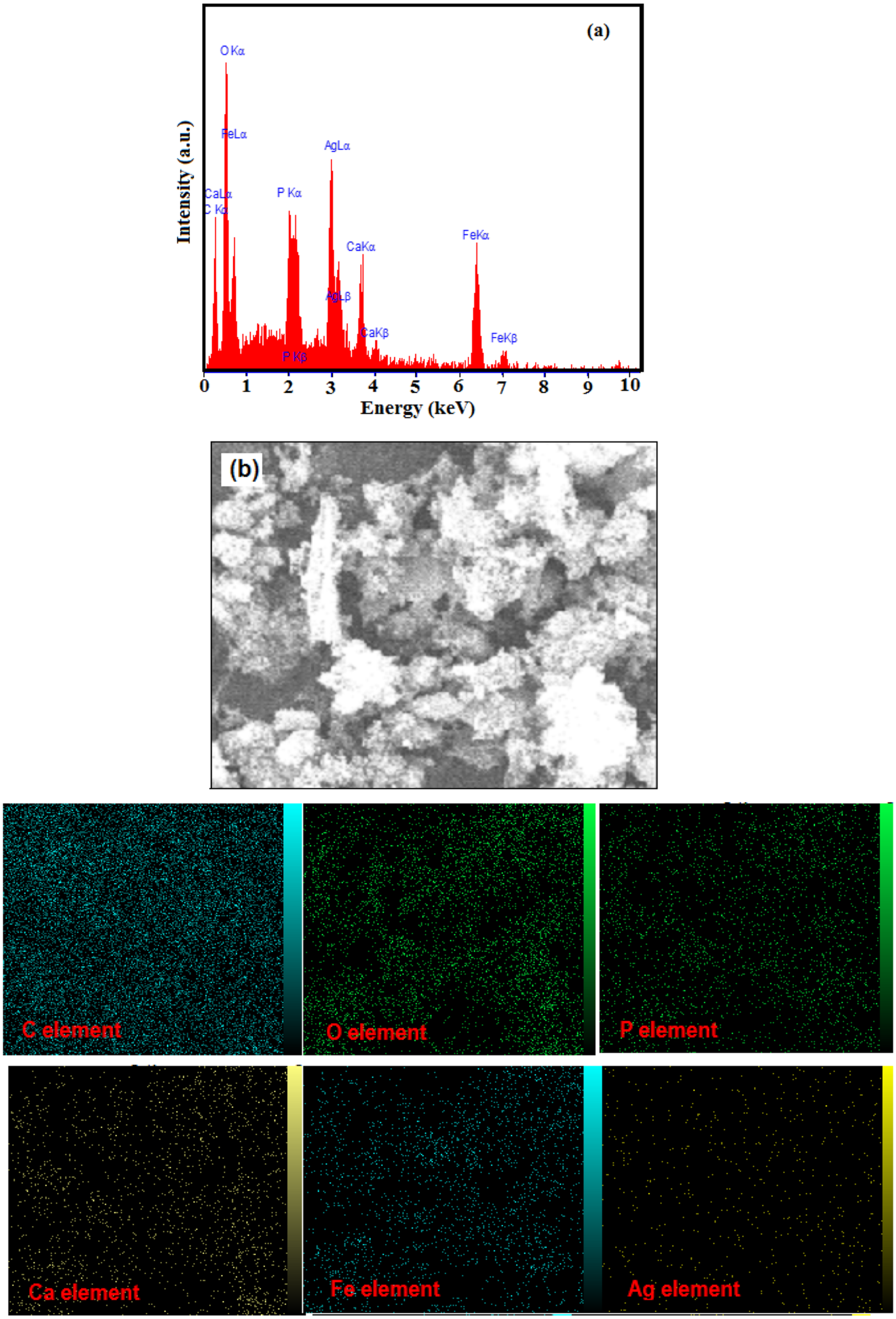

Fig. 5 (a) EDX spectrum and (b) SEM image and the corresponding elemental mappings of the HAP/MIL-101(Fe)/Ag/Fe_3O_4 nanocomposite.

assigned to the ν_3 P–O asymmetric stretching vibrations and the peaks at 567, 603 cm^{-1} were attributed to the ν_4 P–O bending vibrations. Also, the weak peaks at 960 and 466 cm^{-1} correspond to the ν_1, ν_2 P–O symmetrical stretching vibrations, respectively. The peak at around 3550 cm^{-1} is ascribed to the stretching vibration of structural O–H, and the peak at 631 cm^{-1} can be attributed to the bending vibration of O–H, confirming the presence of OH^- groups in the synthesized HAP.[30,31] For

© 2023 The Author(s). Published by the Royal Society of Chemistry

Open Access Article. Published on 04 May 2023. Downloaded on 1/18/2026 3:06:55 PM.
This article is licensed under a Creative Commons Attribution-NonCommercial 3.0 Unported Licence.

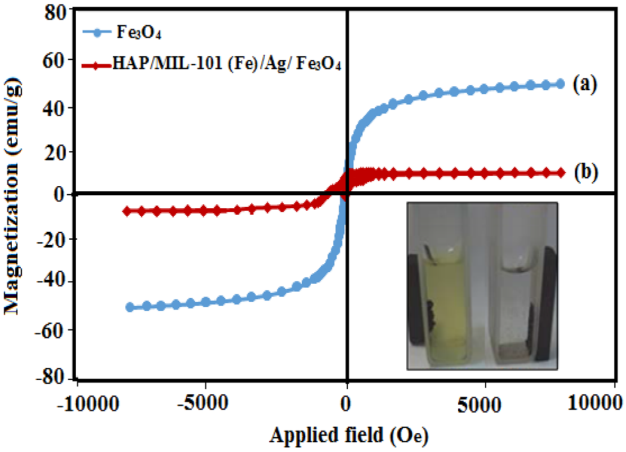

Fig. 6 Magnetic hysteresis loops of (a) pure Fe_3O_4 and (b) HAP/MIL-101(Fe)/Ag/Fe_3O_4 nanocomposite at room temperature.

MIL-101(Fe) sample in Fig. 1(b), the two strong peaks at 1598 and 1390 cm^{-1} are assigned to the symmetric and asymmetric stretching of carboxyl groups (O–C–O) in H_2BDC, respectively. The peak at 750 cm^{-1} is specified as the out-of-plane C–H bending vibration in ring benzene of H_2BDC. Moreover, the apparent peak at 540 cm^{-1} indicated the Fe–O vibration.[24,29] In Fig. 1(c), the intrinsic peak at 572 cm^{-1} relates to the Fe–O bond vibration of Fe_3O_4.[24] The FT-IR spectra of the nanocomposites are shown in Fig. 1(d)–(f). All the nanocomposites showed characteristic peaks relating to HAP and MIL-101(Fe), which confirms the successful synthesis of nanocomposites. No peak of Ag NPs can be observed in the FT-IR spectrum. In Fig. 1(f), the Fe_3O_4 peak could not be recognized because the characteristic Fe–O band at 572 cm^{-1} overlapped with the phosphate peaks of HAP at 567 and 603 cm^{-1}.

The phase purity and crystalline structure of the pure HAP, MIL-101(Fe), Fe_3O_4, HAP/MIL-101(Fe), HAP/MIL-101(Fe)/Ag, and HAP/MIL-101(Fe)/Ag/Fe_3O_4 nanocomposites were investigated *via* XRD analysis and the corresponding spectra are indicated in Fig. 2. In Fig. 2(a), diffraction peaks of pure HAP appeared at 2θ around 25.9°, 32°, 33°, 34.1°, 39.8°, 46.7°, and 50°, corresponding to the (002), (211), (300), (202), (310), (222), and (321) planes (JCPDS card no. 09-0432). These peaks indicate the hexagonal phase of HAP crystals.[21] The XRD pattern of MIL-101(Fe) in Fig. 2(b) showed characteristic peaks at $2\theta = 9.7°$, 16.7°, and 18.9°, which are assigned to the (119), (115), and (224) planes, respectively.[24] From Fig. 2(c), the main diffraction

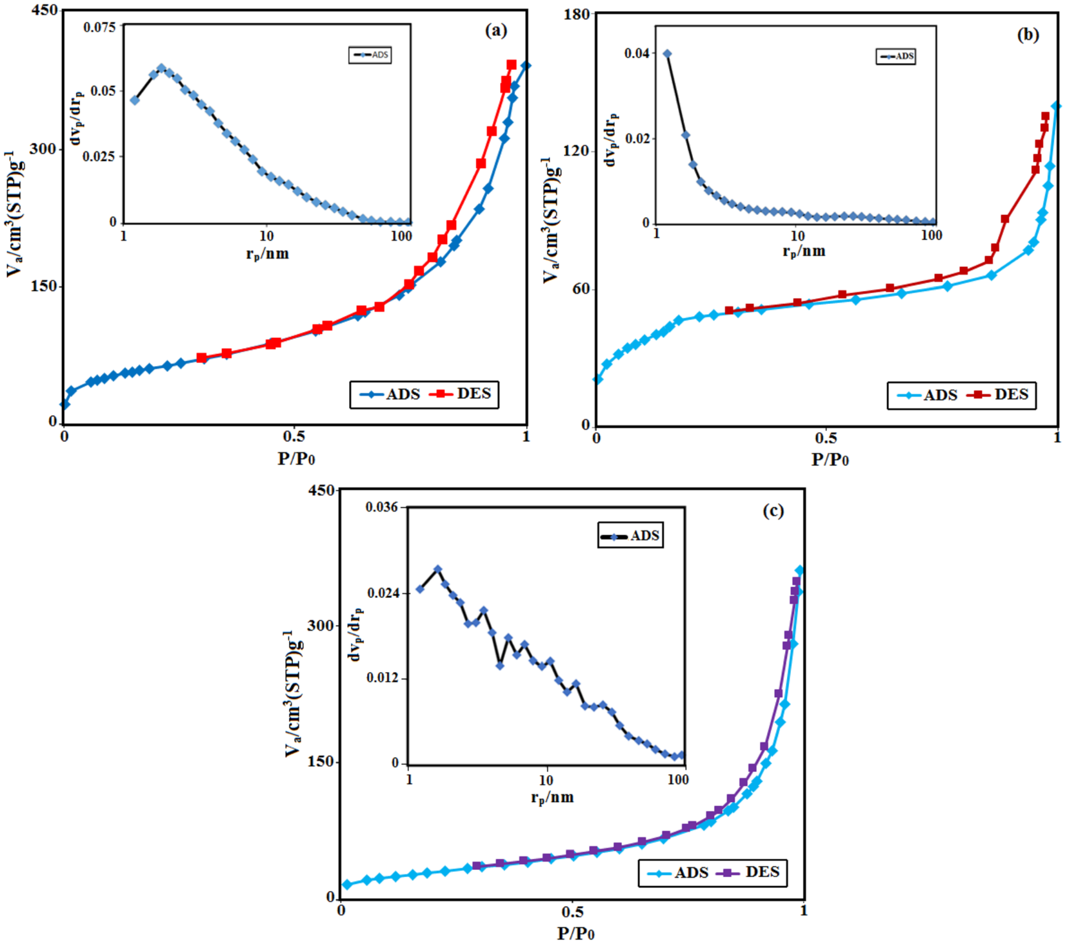

Fig. 7 Nitrogen adsorption–desorption isotherms and pore-size distribution curves (the insets) of (a) pure HAP, (b) pure MIL-101(Fe), and (c) the HAP/MIL-101(Fe)/Ag/Fe_3O_4 nanocomposite.

Open Access Article. Published on 04 May 2023. Downloaded on 1/18/2026 3:06:55 PM.
This article is licensed under a Creative Commons Attribution-NonCommercial 3.0 Unported Licence.

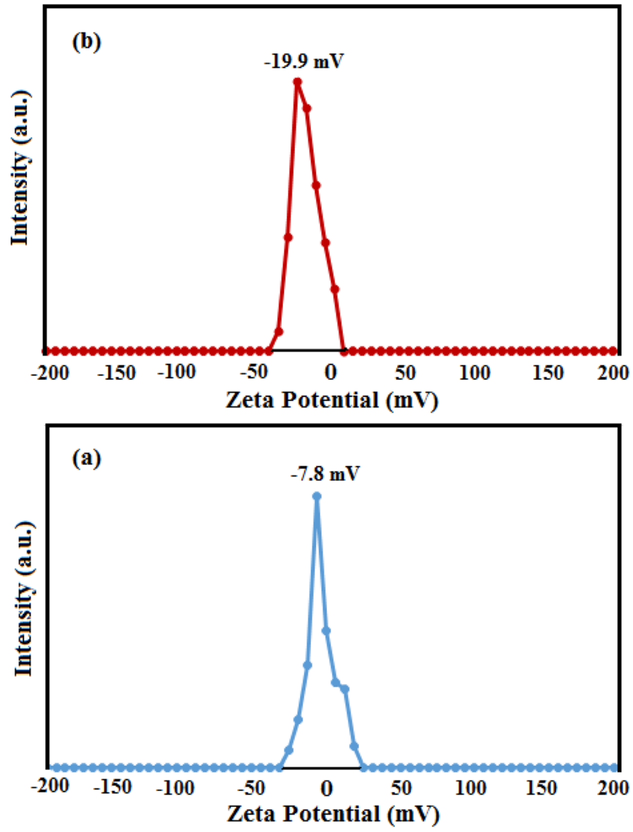

Fig. 8 Zeta potential curves of (a) pure HAP and (b) HAP/MIL-101(Fe)/Ag/Fe_3O_4 nanocomposite in water at natural pH.

peaks of Fe_3O_4 particles are observed at $2\theta = 30.2°$, 35.6°, 43.3°, 53.7°, 57.3°, and 62.8°, corresponding to (220), (311), (400), (422), (511), and (440) the crystal planes (JCPDS card No. 19-0629).[32] The XRD patterns of the nanocomposites are shown in Fig. 2(d)–(f). The sharp diffraction peaks of hexagonal HAP and MIL-101(Fe) can be found in all nanocomposites. In addition, peaks related to pure Ag NPs were also observed in the HAP/MIL-101(Fe)/Ag and HAP/MIL-101(Fe)/Ag/Fe_3O_4 nanocomposites. These peaks were observed at $2\theta = 38.1°$, 44.3°, 64.4°, and 77.5°, corresponding to the (111), (200), (220), and (311) planes that represent the face-centered cubic (fcc) structures of Ag NPs (JCPDS, card no. 87-0717).[33] However, compared to the pure HAP, the diffraction peak intensity of HAP in the HAP/MIL-101(Fe)/Ag/Fe_3O_4 nanocomposite appears slightly reduced, confirming the successful loading of MIL-101(Fe), Ag, and Fe_3O_4 nanoparticles on the surface HAP.

The Raman technique was employed to complete the structural analysis and detection of HAP, MIL-101(Fe), and HAP/MIL-101(Fe)/Ag/Fe_3O_4 nanocomposite. As shown in Fig. 3(a), the pure HAP presented peaks at 470 (ν_2), 572 (ν_4), 960 (ν_1), and 1035 cm^{-1} (ν_3), which refer to the vibration modes of the tetrahedral phosphate groups, respectively.[21] For the MIL-101(Fe) sample in Fig. 3(b), the vibrational bands observed at 862, 1138, 1292, 1431, 1504, and 1613 cm^{-1} related to the dicarboxylate and aromatic groups in H_2BDC.[34] Based on Fig. 3(c), the HAP/MIL-101(Fe)/Ag/Fe_3O_4 nanocomposite showed adsorption bands relating to HAP but in weaker intensities along with the characteristic peaks of MIL-101(Fe) and Fe_3O_4 nanoparticles, confirming the formation of the final nanocomposite.

The size and surface morphologies of HAP and HAP/MIL-101(Fe)/Ag/Fe_3O_4 nanocomposite were carried out using two techniques, SEM and TEM. As shown in Fig. 4(a), HAP consists of uniform rods with lengths of 90–232 nm and widths of 29–56 nm. The nanocomposite has a rod-like structure with a length of 2200 nm and a width of 678 nm (Fig. 4(b) and (c)). In fact, the size of rods in the HAP/MIL-101(Fe)/Ag/Fe_3O_4 nanocomposite was considerably increased after growing a layer of MIL-101(Fe) on them. From Fig. 4(a), it is clearly found that HAP has a relatively smooth surface. However, as can be seen in Fig. 4(b) and (c), the SEM images show that the nanocomposite possesses rough structures with a large amount of well-dispersed sphere-like nanoparticles on the surface, which can be clearly observed from the TEM images in Fig. 4(d) and (e).

The EDX spectrum and SEM image, together with the corresponding elemental mappings of the HAP/MIL-101(Fe)/Ag/Fe_3O_4 nanocomposite, are shown in Fig. 5(a) and (b), respectively. The EDX spectrum clearly showed the presence of Ca, P, C, Ag, O, and Fe elements in the nanocomposite without any other elements, confirming the synthesis of the nanocomposite. In addition, the EDX elemental mapping also detected all of the six main elements (*i.e.*, Ca, P, C, Ag, O, and Fe) in the nanocomposite without any other impurities.

The magnetic hysteresis loops of pure Fe_3O_4 and HAP/MIL-101(Fe)/Ag/Fe_3O_4 nanocomposite were investigated using a vibrating sample magnetometer with the applied magnetic field ranging from −10 000 to 10 000 Oe at room temperature. Fig. 6(a) and (b) indicate that the saturation magnetization (Ms) value for the nanocomposite is 15 emu g^{-1}, which is lower than that of Fe_3O_4 nanoparticles (72 emu g^{-1}). The decrease in magnetization of the nanocomposite can be due to the density decrease of magnetic Fe_3O_4 nanocrystals in the HAP/MIL-101(Fe)/Ag/Fe_3O_4 nanocomposite. The magnetization of synthesized HAP/MIL-101(Fe)/Ag/Fe_3O_4 nanocomposite is strong enough that it can be quickly attracted by an external magnetic field.

The nitrogen adsorption–desorption isotherms and BJH pore size distribution curves of HAP, MIL-101(Fe), and HAP/MIL-101(Fe)/Ag/Fe_3O_4 samples are shown in Fig. 7. The average pore diameters of 10.62, 4.75, 18.88 nm were obtained for pure HAP, MIL-101(Fe) and HAP/MIL-101(Fe)/Ag/Fe_3O_4, respectively. The samples showed type IV isotherms with the hysteresis loops of H_3 type ascribed to their mesoporous structure, which was also confirmed by the obtained average pores diameter. The BET analysis displayed that the specific surface area of HAP/MIL-101(Fe)/Ag/Fe_3O_4 was 112.24 m^2 g^{-1}, respectively, which was smaller than that of the pure HAP (223.50 m^2 g^{-1}) and MIL-101(Fe) (166.97 m^2 g^{-1}). It can be concluded that the loading of Ag and Fe_3O_4 nanoparticles onto the surface of HAP/MIL-101(Fe) leads to the occupation of pores and decrease the porosity. Due to the dispersion of Ag NPs onto the HAP/MIL-101(Fe) network, they show high catalytic activity.

© 2023 The Author(s). Published by the Royal Society of Chemistry

Open Access Article. Published on 04 May 2023. Downloaded on 1/18/2026 3:06:55 PM.
This article is licensed under a Creative Commons Attribution-NonCommercial 3.0 Unported Licence.

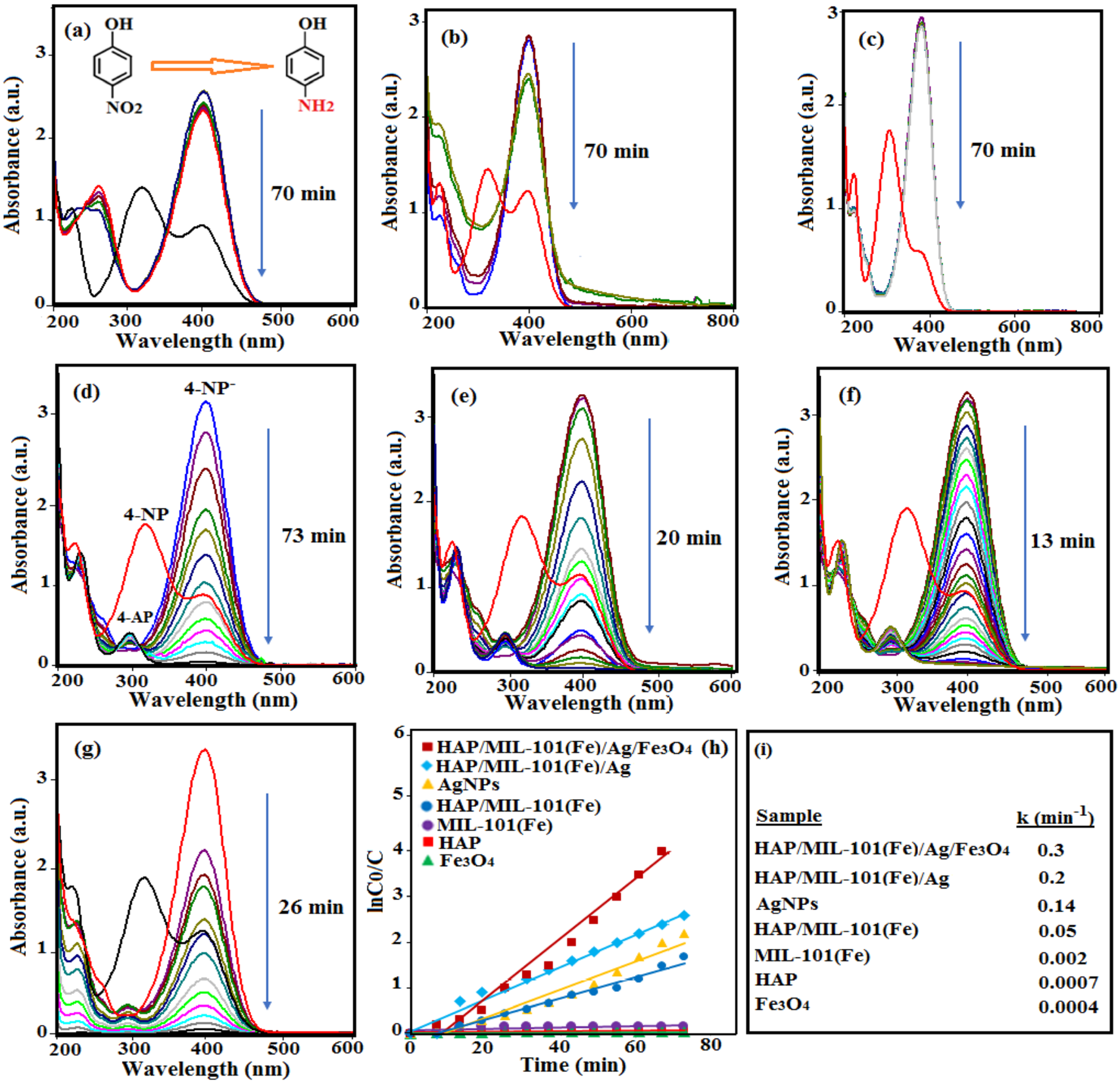

Sample	k (min^{-1})
HAP/MIL-101(Fe)/Ag/Fe$_3$O$_4$	0.3
HAP/MIL-101(Fe)/Ag	0.2
AgNPs	0.14
HAP/MIL-101(Fe)	0.05
MIL-101(Fe)	0.002
HAP	0.0007
Fe$_3$O$_4$	0.0004

Fig. 9 UV-vis absorption spectra of 4-NP reduction using $NaBH_4$ in the presence of (a) pure HAP, (b) MIL-101(Fe), (c) Fe_3O_4, (d) HAP/MIL-101(Fe), (e) HAP/MIL-101(Fe)/Ag, (f) HAP/MIL-101(Fe)/Ag/Fe_3O_4 (g) AgNPs as a catalyst and (h) plots of $\ln(C_0/C_t)$ *versus* the reaction time (i) the apparent rate constant values. Reaction conditions: 4-NP (2 mL, 0.2 mM), $NaBH_4$ (0.5 mL, 20 mM), catalyst (5 mg) and $T = 25$ °C.

Zeta potential is an essential parameter to evaluate the surface charges of the nanoparticles and the electrostatic interaction between the nanoparticles and pollutants. Zeta potential measurements of the as-obtained samples were performed in water at natural pH (pH ≈ 7), and the results are shown in Fig. 8. Zeta potential values of pure HAP and HAP/MIL-101(Fe)/Ag/Fe_3O_4 nanocomposite were −7.8 and −19.9 mV, respectively.

3.2. Catalytic activity of HAP/MIL-101(Fe)/Ag/Fe_3O_4 nanocomposite

The catalytic reduction reaction of 4-NP was investigated over the HAP/MIL-101(Fe)/Ag/Fe_3O_4 nanocomposite as the catalyst and $NaBH_4$ as a reducing agent in an aqueous medium. Fig. 9(a)–(g) displays the UV-visible spectra of 4-NP in the presence of pure HAP, Fe_3O_4, MIL-101(Fe), HAP/MIL-101(Fe), Ag NPs, HAP/MIL-101(Fe)/Ag HAP/MIL-101(Fe)/Ag/Fe_3O_4 nanocomposite with $NaBH_4$. The characteristic peak of 4-NP appeared at 317 nm. After adding alkaline $NaBH_4$ into the solution, due to the formation of 4-nitrophenolate ions, the absorption peak of 4-NP shifted to 400 nm.[9,33] The absorption maximum at 400 nm remained unchanged with the passage of time and without adding the catalyst. When 5 mg of HAP/MIL-101(Fe)/Ag/Fe_3O_4 catalyst was added into the 4-NP solution, the absorption intensity at 400 nm decreased quickly. Simultaneously, a new peak at 297 nm was created, corresponding to 4-AP. The reduction reaction of 4-NP was completed within 13 min, and it was indicated by the disappearance of the yellow color of the reaction solution. According to Fig. 9(a)–(g), pure HAP, Fe_3O_4, MIL-101(Fe), HAP/MIL-101(Fe), Ag NPs, and HAP/MIL-101(Fe)/Ag exhibited lower ability for the reduction of 4-NP compared to the HAP/MIL-101(Fe)/Ag/Fe_3O_4 nanocomposite. The existence of Fe_3O_4 nanoparticles in the

Open Access Article. Published on 04 May 2023. Downloaded on 1/18/2026 3:06:55 PM.
This article is licensed under a Creative Commons Attribution-NonCommercial 3.0 Unported Licence.

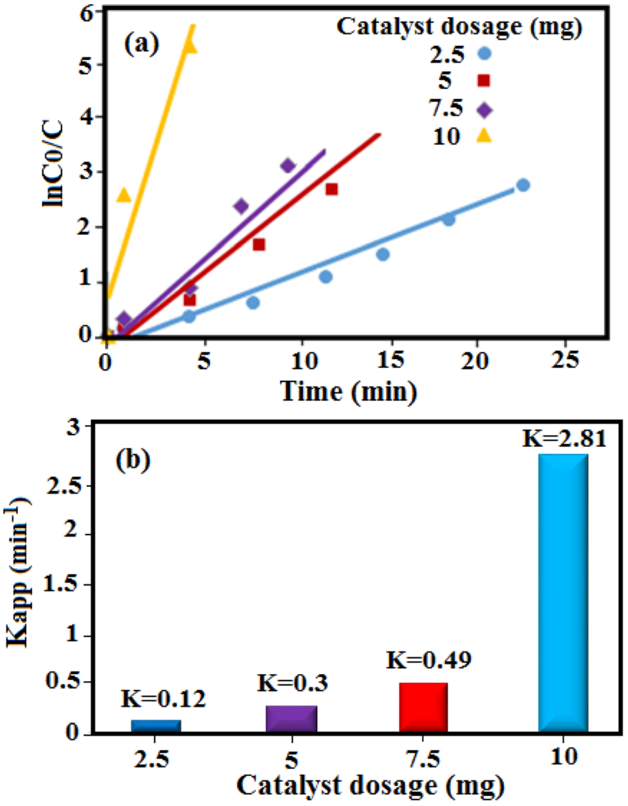

Fig. 10 (a) Plots of ln(C_0/C_t) *versus* the reaction time for 4-NP reduction with $NaBH_4$ in the presence of different amounts of HAP/MIL-101(Fe)/Ag/Fe_3O_4 catalyst and (b) the apparent rate constant values. Reaction conditions: 4-NP (2 mL, 0.2 mM), $NaBH_4$ (0.5 mL, 20 mM), and T = 25 °C.

composite improves the catalytic ability. In addition, it makes it easier to separate the composite from the reaction mixture. Therefore, HAP/MIL-101(Fe)/Ag/Fe_3O_4 nanocomposite was considered an effective catalyst, and other reactions were investigated in the presence of this catalyst.

Since the concentration of $NaBH_4$ is much high compared to that of 4-NP, its concentration remains constant during the reaction. Therefore, the reaction rate can be measured only by the concentration of 4-NP, and the reduction reaction is considered as pseudo-first order kinetic. This equation can be shown as $\ln C_0/C_t = k_{app}t$, where C_0 and C_t refer to the concentration of 4-NP at time 0 and t, respectively. k_{app} and t are the apparent rate constant and the reaction time, respectively. As shown in Fig. 9(h), from the $\ln C_0/C_t$ *versus* time plots, the rate constant (k_{app}) values can be calculated. The rate constants (k_{app}) for the reduction of 4-NP with $NaBH_4$ over pure HAP, Fe_3O_4, MIL-101(Fe), HAP/MIL-101(Fe), Ag NPs, HAP/MIL-101(Fe)/Ag, and HAP/MIL-101(Fe)/Ag/Fe_3O_4 nanocomposite were calculated to be 0.0007, 0.0004, 0.002, 0.05, 0.14, 0.2, and 0.3 min^{-1}, respectively.

According to the results obtained, the synthesized HAP/MIL-101(Fe)/Ag/Fe_3O_4 quaternary nanocomposite showed the highest catalytic activity in the reduction of 4-nitrophenol as compared with each component and even the binary composite. This high catalytic activity of the composite is due to the distribution of Ag NPs in the porous structures of HAP and MIL-101(Fe) and the synergistic effect of the composite components. Due to their porous structure and high surface area, HAP and MIL-101(Fe) provide more space for Ag NPs to perform the 4-nitrophenol reduction reaction and prevents the aggregation of Ag NPs, which reduces its catalytic performance.[35,36]

The mechanism of reaction for the reduction of 4-NP by the HAP/MIL-101(Fe)/Ag/Fe_3O_4 catalyst is as follows: in this reaction, first 4-NP and BH_4^- ions are adsorbed on the surface of the catalyst. During the reduction process, hydride ions are also released by BH_4^- and react with water protons to produce H_2 molecules. These molecules are converted to active hydrogen atoms on the surface of the catalyst. The active hydrogen atoms attack the 4-NP molecule and then the Ag nanoparticles, as an electron and hydrogen mediator, transfer electrons and hydrogen from BH_4^- to 4-NP, finally leading to the formation of 4-AP.[37,38] Because amino groups have a much weaker adsorption ability than nitro groups, the produced 4-AP is desorbed from the catalyst surface. The influence of the catalyst dosage on the catalytic efficiency was studied in the range of 2.5–10 mg. It was found that the catalytic efficiency increases with the increase in the catalyst dosage. Increasing the catalyst dosage provides more active sites on the catalyst surface for the reaction, which in turn increases the production of H_2 and e^- from $NaBH_4$, finally leading to an increase in the reaction rate. Plots of $\ln C_0/C_t$ *versus* reaction time and rate constants for the reduction of 4-NP using different amounts of HAP/MIL-101(Fe)/Ag/Fe_3O_4 catalyst are portrayed in Fig. 10(a) and (b), respectively.

Catalytic reduction of other nitroaromatic compounds such as 2-nitrophenol (2-NP), 2,4-dinitrophenol (2,4-NP), 4-nitroaniline (4-NA), and 2-nitroaniline (2-NA) was carried out using HAP/MIL-101(Fe)/Ag/Fe_3O_4 and $NaBH_4$ in aqueous solution, as shown in Fig. 11(a)–(d). The absorbance peak for these three compounds was also observed at about 400 nm under alkaline conditions. The absorption peaks of 2-NP, 2,4-NP, 4-NA, and 2-NA were decreased in 8, 32, 18, and 10 min, respectively. Fig. 11(e) shows the rate constant values obtained for these compounds.

Comparison between the obtained results to the reduction of 4-NP in the presence of HAP/MIL-101(Fe)/Ag/Fe_3O_4 catalyst and $NaBH_4$ with other reported catalysts is indicated in Table 1.[39–52] From Table 1, it can be seen that the reaction in the presence of the HAP/MIL-101(Fe)/Ag/Fe_3O_4 catalyst required a shorter reaction time compared with most of the reported catalysts, which confirms the potential of the current catalyst for the reduction of 4-nitrophenol in aqueous solutions.

3.3. Antibacterial activity of the HAP/MIL-101(Fe)/Ag/Fe_3O_4 nanocomposite

Among the various nanoparticles that are known as antimicrobial agents, Ag NPs have been widely studied. Ag NPs can be effective in killing various types of viruses, bacteria, fungi, and other pathogenic microbes. However, the antibacterial ability of Ag NPs is decreased due to problems related to their agglomeration.[53] Thus, nanocomposites composed of Ag NPs with

© 2023 The Author(s). Published by the Royal Society of Chemistry

Open Access Article. Published on 04 May 2023. Downloaded on 1/18/2026 3:06:55 PM.
This article is licensed under a Creative Commons Attribution-NonCommercial 3.0 Unported Licence.

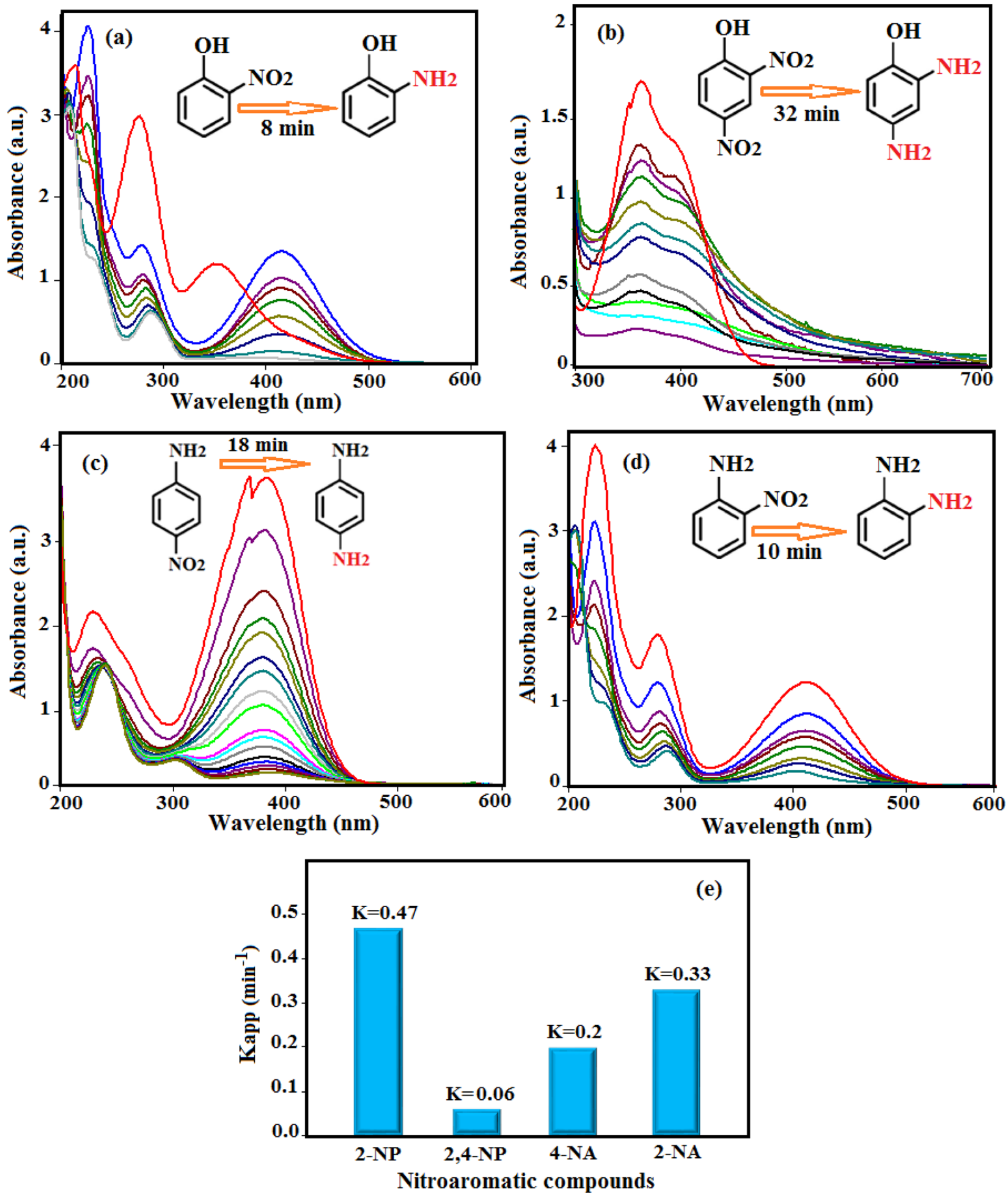

Fig. 11 UV-vis absorption spectra for the reduction reaction of (a) 2-NP, (b) 2,4-NP, (c) 4-NA, and (d) 2-NA with $NaBH_4$ in the presence of HAP/MIL-101(Fe)/Ag/Fe_3O_4 catalyst. (e) The apparent rate constant values. Reaction conditions: nitro compound (2 mL, 0.2 mM), $NaBH_4$ (0.5 mL, 20 mM), catalyst (5 mg), and T = 25 °C.

other materials, such as HAP, graphene (GO), carbon nanotubes (CNTs), *etc.*, have been prepared and tested against different bacterial strains.[54,55] The antibacterial abilities of the prepared HAP/MIL-101(Fe)/Ag/Fe_3O_4 nanocomposite and Ag NPs were investigated by disk diffusion method, using a Gram-negative bacterium (*Escherichia coli*) and two Gram-positive bacteria (*Staphylococcus saprophyticus* and *Staphylococcus aureus*). Fig. 12(a) and (b) and Table 2 show the results of this investigation at the concentration of 40 μg mL^{-1}. According to Table 2, HAP/MIL-101(Fe)/Ag/Fe_3O_4 nanocomposite and Ag NPs were effective against all tested bacterial strains. Overall, the HAP/MIL-101(Fe)/Ag/Fe_3O_4 nanocomposite and Ag NPs demonstrated the lowest antibacterial activity against *Escherichia coli*, and the higher antibacterial activity of the HAP/MIL-101(Fe)/Ag/Fe_3O_4 nanocomposite and Ag NPs was obtained against *Staphylococcus saprophyticus* and *Staphylococcus aureus*. Moreover, as expected, HAP/MIL-101(Fe)/Ag/Fe_3O_4 nanocomposite exhibited higher antibacterial ability than the Ag NPs. The antibacterial effects of pure HAP, MIL-101(Fe), and HAP/MIL-101(Fe) samples were also tested, and no significant antibacterial activity was observed against bacterial species. The mechanism of antibacterial activity of Ag NPs from the point of view of molecular microbiology is not yet fully known. However, some of its main mechanisms are as follows: first, Ag NPs

Open Access Article. Published on 04 May 2023. Downloaded on 1/18/2026 3:06:55 PM.
This article is licensed under a Creative Commons Attribution-NonCommercial 3.0 Unported Licence.

Table 1 Comparison of the catalytic activity of HAP/MIL-(Fe)/Ag/Fe_3O_4 with different reported catalysts for the complete reduction (100%) of 4-NP

Catalyst	Reaction conditions	Time (min)	Ref.
Ag NPs	H_2O, $NaBH_4$, r.t.	15	39
Au NPs	H_2O, $NaBH_4$, r.t.	30	40
Ni–ZnO NWA@SSM	H_2O, $NaBH_4$, r.t.	30	41
MoS_2/ZnO	H_2O, $NaBH_4$, r.t.	15	42
Pd/rGO-H	H_2O, $NaBH_4$, r.t.	60	43
Ni_2P/BC	H_2O, $NaBH_4$, r.t.	3	44
Ni/NiO	H_2O, $NaBH_4$, r.t.	45	45
GO/Ag NPs	H_2O, $NaBH_4$, r.t.	20	46
Co_3O_4/HNTs	H_2O, $NaBH_4$, r.t.	11	47
CuO/C	H_2O, $NaBH_4$, r.t.	18	48
g-C_3N_4/Ag_2S	H_2O, $NaBH_4$, r.t.	42	49
TOCNF-ZiF67@FP	H_2O, $NaBH_4$, r.t.	5	50
1T-MoS_2/PC	H_2O, $NaBH_4$, r.t.	15	51
HAP/Cu NPs	H_2O, $NaBH_4$, r.t.	8	52
HAP/MIL-101(Fe)/Ag/Fe_3O_4	H_2O, $NaBH_4$, r.t.	13	This work

gradually release Ag^+ ions from themselves. Since Ag^+ ions have a positive charge, they are drawn towards the negatively charged bacterial cell wall and permeate the cells. After the permeation of Ag^+ ions into cells, these ions connect with cellular structures and biological molecules such as proteins, lipids, and DNA, thus damaging the internal structure of bacteria.[56] Ag NPs interact with sulfur-containing proteins (for example, with the thiol group of the respiratory chain protein) and cause the inactivation of bacterial enzymes. Also, Ag NPs can interact with bacterial DNA and disrupt its replication ability, which finally leads to the death of bacteria.[57–59] On the other hand, the lower

Table 2 Average inhibition zone of the nanocomposite and AgNPs against bacteria

		Inhibition zone diameter (mm)	
Bacteria	Type	Nanocomposite	Ag NPs
S. aureus	Gram-positive	17 ± 0.65	13 ± 0.73
S. saprophyticus	Gram-positive	14 ± 0.43	11 ± 0.36
E. coli	Gram-negative	12 ± 0.56	9 ± 0.48

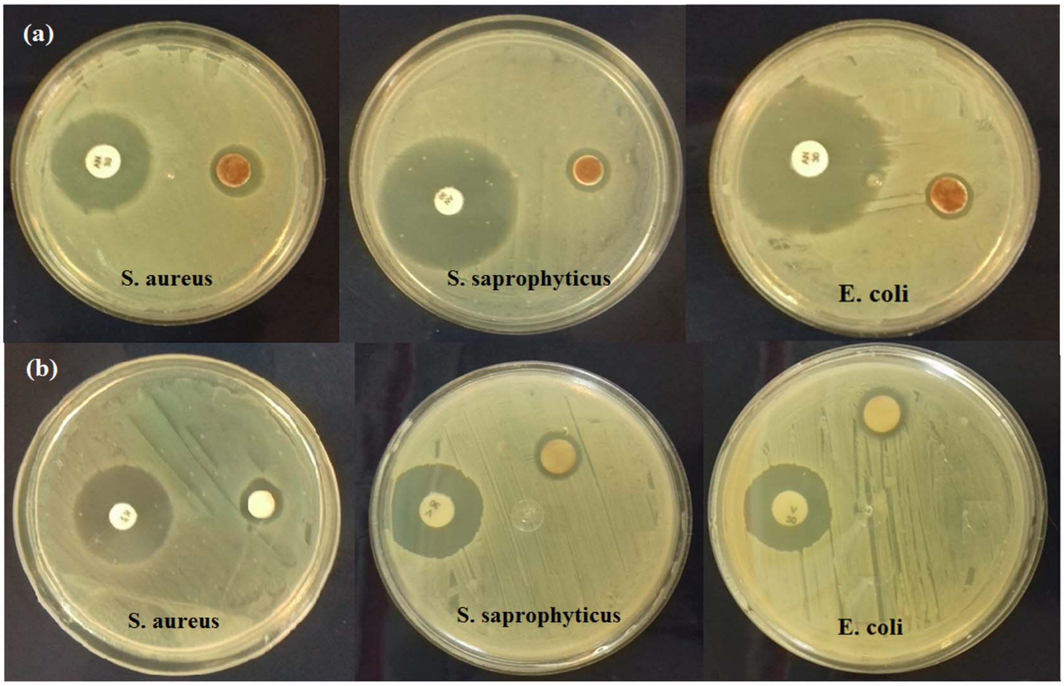

Fig. 12 The images of the antibacterial ability of disc 40 μg mL^{-1} HAP/MIL-101(Fe)/Ag/Fe_3O_4 nanocomposite (a) and Ag NPs (b) against different bacterial strains.

Open Access Article. Published on 04 May 2023. Downloaded on 1/18/2026 3:06:55 PM.
This article is licensed under a Creative Commons Attribution-NonCommercial 3.0 Unported Licence.

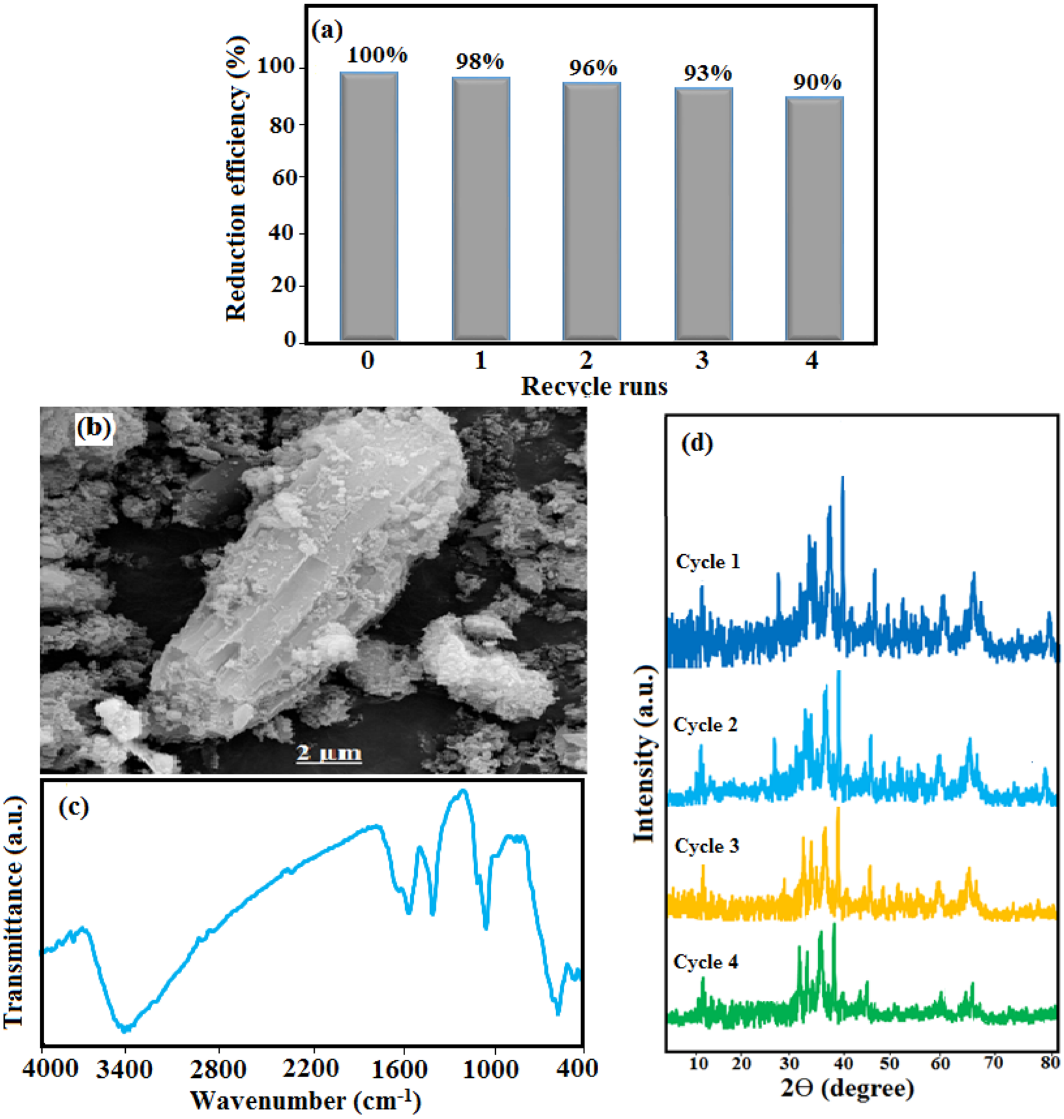

Fig. 13 (a) The reusability of the HAP/MIL-101(Fe)/Ag/Fe_3O_4 catalyst for the reduction of 4-NP, (b) SEM image, (c) FT-IR spectrum of the catalyst after the fourth cycle, and (d) XRD patterns of the recovered catalyst after 1st–4th cycles.

sensitivity of Gram-negative *Escherichia coli* to Ag NPs can be due to the outer membrane of this bacterium, which is mainly composed of stable lipopolysaccharide and is considered as a resistant barrier against Ag NPs. Furthermore, the greater sensitivity of Gram-positive bacteria such as *Staphylococcus saprophyticus* and *Staphylococcus aureus* to Ag NPs has been ascribed to the greater abundance of carboxyl, thiol, and amine functional groups on their cell surface and strong affinity of these groups to combine with Ag^+ ions.[60] In addition, the interaction of Ag NPs with bacteria also depends on the shape, size, dose, and diffusion rate.

3.4. Reusability of the HAP/MIL-101(Fe)/Ag/Fe_3O_4 nanocomposite

The stability and reuse of the prepared catalyst for practical applications as well as cost reduction are important issues that have been considered. For this purpose, after the completion of the reaction, an external magnet was used to separate the HAP/MIL-101(Fe)/Ag/Fe_3O_4 catalyst from the reaction solution. The catalyst containing 4-nitrophenol was dissolved in 50 mL ethanol and stirred for 6 h at room temperature. Then, it was filtered, dried at 70 °C for 12 h, and used for the next cycle. The results in Fig. 13(a) showed that the decrease in the catalytic efficiency was not significant for four successive cycles. The reduction of 4-NP reached 90% after four cycles. At the same time, the amounts of leached Ag NPs in the clear filtrate solutions of 4-NP after four cycles of 4-NP reduction experiments were determined to be in the range of 0.1–0.15% by ICP-AES analysis. The results showed that the amount of leached Ag from the catalyst is not noticeable, confirming the stability of the catalyst. In addition, the hot filtration test was performed by taking the catalyst out of the mixture 6 min after the reaction. The reduction efficiency of 4-NP over 13 min was almost constant, which indicates that the catalyst is truly

Open Access Article. Published on 04 May 2023. Downloaded on 1/18/2026 3:06:55 PM.
This article is licensed under a Creative Commons Attribution-NonCommercial 3.0 Unported Licence.

heterogeneous. On the other hand, SEM and FT-IR analyses proved the structural stability of the recovered catalyst after four cycles, as shown in Fig. 13(b) and (c). As shown in Fig. 13(d), XRD patterns of the catalyst after recovering from the first run to the fourth run did not show significant changes in comparison with the fresh catalyst in Fig. 2(f). Therefore, the as-prepared nanocomposite catalyst can work as an effective catalyst for the reduction of nitroaromatic compounds with good stability, high crystallinity, and recyclability.

4. Conclusion

In this study, a novel quaternary nanocomposite was successfully synthesized through several step reactions for the first time. The results obtained from FT-IR, XRD, Raman, SEM, EDX, and TEM analyses confirmed that MIL-101(Fe) and Ag and Fe_3O_4 nanoparticles are distributed on the surface of HAP. The catalytic efficiency of the HAP/MIL-101(Fe)/Ag/Fe_3O_4 nanocomposite for the reduction of 4-nitrophenol and other nitroarenes was excellent, and no side products were formed. In addition, the nanocomposite showed good antibacterial activity against the tested bacterial strains due to the presence of Ag NPs. Also, due to the super-paramagnetic property of Fe_3O_4 nanoparticles, this nanocomposite can be easily and quickly collected using a magnet after the reduction process and reused up to four times without any significant change in performance and efficiency.

Conflicts of interest

There are no conflicts to declare.

Acknowledgements

The authors sincerely thank Lorestan University and Iran Nanotechnology Initiative Council (INIC) for all the support provided.

References

1 M. Saxena, K. Jain and R. Saxena, *Indian J. Biochem. Biophys.*, 2022, **59**, 415–430.
2 H. Singh and J. K. Rajput, *J. Iran. Chem. Soc.*, 2019, **16**, 2409–2432.
3 M. Liu, R. Wang, B. Liu, F. Guo and L. Tian, *J. Colloid Interface Sci.*, 2019, **555**, 423–430.
4 S. D. Ashrafi, G. H. Safari, K. Sharafi, H. Kamani and J. Jaafari, *Int. J. Biol. Macromol.*, 2021, **185**, 66–76.
5 H. Ali and A. M. Ismail, *J. Polym. Environ.*, 2022, **30**, 3379–3390.
6 W. Raza, K. Ahmad and H. Kim, *Nanotechnology*, 2021, **32**, 495404.
7 Z. M. Shammi, A. H. Kianfar and M. M. Momeni, *J. Mater. Sci. Mater. Electron.*, 2020, **31**, 14810–14822.
8 M. T. Nakhjiri, G. Bagheri Marandi and M. Kurdtabar, *J. Environ. Chem. Eng.*, 2021, **9**, 105039.
9 M. Riaz, U. Sharafat, N. Zahid, M. Ismail, J. Park, B. Ahmad, N. Rashid, M. Fahim, M. Imran and A. Tabassum, *ACS Omega*, 2022, **7**, 14723–14734.
10 S. Chatterjee, M. Chakraborty, K. K. Bera, A. Mahajan, S. Banik, P. S. Roy and S. K. Bhattacharya, *IOP Conf. Ser. Mater. Sci. Eng.*, 2021, **1080**, 012010.
11 P. Zarringhadam and S. Farhadi, *Acta Chim. Slov.*, 2018, **65**, 448–461.
12 P. Cyganowski and J. Wolska, *React. Funct. Polym.*, 2022, **170**, 105119.
13 G. Grieco and O. Blacque, *Appl. Organomet. Chem.*, 2022, **36**, 1–13.
14 E. M. Bakhsh, M. Ismail, U. Sharafat, K. Akhtar, T. M. Fagieh, E. Y. Danish, S. B. Khan, M. I. Khan, M. A. Khan and A. M. Asiri, *J. Mater. Res. Technol.*, 2022, **18**, 769–787.
15 M. Arif, M. Shahid, A. Irfan, J. Nisar, W. Wu, Z. H. Farooqi and R. Begum, *RSC Adv.*, 2022, **12**, 5105–5117.
16 L. Huang, Y. Lv, S. Wu, P. Liu, W. Xiong, F. Hao and H. Luo, *Appl. Catal., A*, 2019, **577**, 76–85.
17 Y. Qu, G. Xu, J. Yang and Z. Zhang, *Appl. Catal., A*, 2020, **590**, 117311.
18 J. Y. Lin, P. Y. Chen, E. Kwon, W. Da Oh, S. You, C. W. Huang, F. Ghanbari, T. Wi-Afedzi and K. Y. A. Lin, *J. Water Process Eng.*, 2021, **40**, 101933.
19 K. Zhang, J. M. Suh, J. W. Choi, H. W. Jang, M. Shokouhimehr and R. S. Varma, *ACS Omega*, 2019, **4**, 483–495.
20 M. Shokouhimehr, *Catalysts*, 2015, **5**, 534–560.
21 G. S. Kumar, G. Karunakaran, E. K. Girija, E. Kolesnikov, N. Van Minh, M. V. Gorshenkov and D. Kuznetsov, *Ceram. Int.*, 2018, **44**, 11257–11264.
22 S. Pai, M. S. Kini and R. Selvaraj, *Environ. Sci. Pollut. Res.*, 2021, **28**, 11835–11849.
23 P. N. Silva-Holguín and S. Y. Reyes-Lopez, *Dose-Response*, 2021, **19**, 1–14.
24 Y. Guo, C. Feng, S. Qiao, S. Wang, T. Chen, L. Zhang, Y. Zhao and J. Wang, *Nanoscale*, 2020, **12**, 12551–12560.
25 G. Zhang, Y. Wang, F. He, L. He, H. Li and D. Xu, *Catal. Commun.*, 2022, **166**, 106454.
26 J. Cai, X. Mao and W. G. Song, *Mater. Chem. Front.*, 2018, **2**, 1389–1396.
27 Y. Dong, T. Hu, M. Pudukudy, H. Su, L. Jiang, S. Shan and Q. Jia, *Mater. Chem. Phys.*, 2020, **251**, 123060.
28 X. Jia, S. Li, Y. Wang, T. Wang and X. Hou, *J. Chem. Eng. Data*, 2019, **64**, 1265–1274.
29 W. Xiong, Z. Zeng, X. Li, G. Zeng, R. Xiao, Z. Yang, Y. Zhou, C. Zhang, M. Cheng, L. Hu, C. Zhou, L. Qin, R. Xu and Y. Zhang, *Chemosphere*, 2018, **210**, 1061–1069.
30 K. W. Jung, S. Y. Lee, J. W. Choi and Y. J. Lee, *Chem. Eng. J.*, 2019, **369**, 529–541.
31 T. Zhang, W. Cai, F. Chu, F. Zhou, S. Liang, C. Ma and Y. Hu, *Composites, Part A*, 2020, **128**, 105681.
32 M. Foroughi, M. H. Ahmadi-Azqhandi and S. Kakhki, *J. Hazard. Mater.*, 2020, **388**, 121769.
33 M. Ahmad, T. Nawaz, M. A. Assiri, R. Hussain, I. Hussain, M. Imran, S. Ali and Z. Wu, *ACS Omega*, 2022, **7**, 7096–7102.
34 A. Jarrah and S. Farhadi, *RSC Adv.*, 2018, **8**, 37976–37992.

© 2023 The Author(s). Published by the Royal Society of Chemistry

Open Access Article. Published on 04 May 2023. Downloaded on 1/18/2026 3:06:55 PM.
This article is licensed under a Creative Commons Attribution-NonCommercial 3.0 Unported Licence.

35 B. Jacob, M. Mohan, K. C. Dhanyaprabha and H. Thomas, *Int. J. Hydrog. Energy*, 2023, **48**, 9285–9305.

36 B. Bhaduri, A. K. Dikshit, T. Y. Kim and K. M. Tripathi, *ACS Appl. Nano Mater.*, 2022, **5**, 16000–16026.

37 J. N. Jebaranjitham, C. Mageshwari, R. Saravanan and N. Mu, *Composites, Part B*, 2019, **171**, 302–309.

38 M. Mahiuddin and B. Ochiai, *Mater. Today Sustainability*, 2023, **5**, 100383.

39 K. K. Bharadwaj, B. Rabha, S. Pati, B. K. Choudhury, T. Sarkar, S. K. Gogoi, N. Kakati, D. Baishya, Z. A. Kari and H. A. Edinur, *Nanomater*, 2021, **11**, 1999.

40 B. Kumar, K. Smita, Y. Angulo, A. Debut and L. Cumbal, *Heliyon*, 2022, **8**, e10191.

41 C. Lin, G. Luo, H. Zhou, A. Feng, L. Zeng and Q. Li, *EcoMat*, 2022, **4**, 1–13.

42 R. J. Madhushree, J. Resnik Jaleel, D. Pinheiro and S. Devi, *Appl. Surf. Sci. Adv.*, 2022, **10**, 100265.

43 T. Zhang, B. Ouyang, X. Zhang, G. Xia, N. Wang, H. Ou, L. Ma, P. Mao, K. Ostrikov, L. Di and X. Tu, *Appl. Surf. Sci.*, 2022, **597**, 153727.

44 Y. Xie, L. Dai, T. Xie, Y. Zhang, Y. Wang and H. Yang, *Chem. Eng. J. Adv.*, 2022, **9**, 100238.

45 A. W. Augustyniak, A. Gniewek, R. Szukiewicz, M. Wiejak, M. Korabik and A. M. Trzeciak, *Polyhedron*, 2022, **224**, 116029.

46 Y. Lu, X. Wan, L. Li, P. Sun and G. Liu, *J. Mater. Res. Technol.*, 2021, **12**, 1832–1843.

47 M. Zhang, X. Su, L. Ma, A. Khan, L. Wang, J. Wang, A. S. Maloletnev and C. Yang, *J. Hazard. Mater.*, 2021, **403**, 123870.

48 A. A. Kassem, H. N. Abdelhamid, D. M. Fouad and S. A. Ibrahim, *J. Environ. Chem. Eng.*, 2021, **9**, 104401.

49 D. Ayodhya and G. Veerabhadram, *J. Mol. Struct.*, 2019, **1186**, 423–433.

50 H. N. Abdelhamid and A. P. Mathew, *Carbohydr. Polym.*, 2021, **274**, 118657.

51 N. Li, Q. Sun, P. Zhang and S. Jing, *Materials*, 2021, **14**, 7020.

52 M. A. El-Aal, H. M. Ali and S. M. Ibrahim, *ACS Omega*, 2022, **7**, 26777–26787.

53 N. Fatima, U. Y. Qazi, A. Mansha, I. A. Bhatti, R. Javaid, Q. Abbas, N. Nadeem, Z. A. Rehan, S. Noreen and M. Zahid, *J. Ind. Eng. Chem.*, 2021, **100**, 40–58.

54 T. T. Thuy, L. Hoang, N. Insin and N. Sukpirom, *Inorg. Chem. Commun.*, 2020, **121**, 108199.

55 N. M. Dat, P. N. B. Long, D. C. U. Nhi, N. N. Minh, L. M. Duy, L. N. Quan, H. M. Nam, M. T. Phong and N. H. Hieu, *Synth. Met.*, 2020, **260**, 116260.

56 X. N. Pham, H. T. Nguyen and N. T. Pham, *Int. J. Biomater.*, 2020, **2020**, 1–12.

57 J. Al-Haddad, F. Alzaabi, P. Pal, K. Rambabu and F. Banat, *Clean Technol. Environ. Policy*, 2020, **22**, 269–277.

58 R. Naaz, W. A. Siddiqi and M. Mohsin, *Orient. J. Chem.*, 2023, **39**, 75–81.

59 R. Naaz, V. U. Siddiqui, A. Ahmad, S. U. Qadir and W. A. Siddiqi, *J. Dispers. Sci. Technol.*, 2023, **5**, 1–11.

60 Y. Qing, L. Cheng, R. Li, G. Liu, Y. Zhang, X. Tang, J. Wang, H. Liu and Y. Qin, *Int. J. Nanomedicine*, 2018, **13**, 3311–3327.

© 2023 The Author(s). Published by the Royal Society of Chemistry